Lipid Interaction Converts Prion Protein to a PrP^{Sc}-like Proteinase K-Resistant Conformation under Physiological Conditions†

Fei Wang,‡ Fan Yang,§ Yunfei Hu,§ Xu Wang,§ Xinhe Wang,‡ Changwen Jin,§ and Jiyan Ma*,‡

Department of Molecular and Cellular Biochemistry, The Ohio State University, Columbus, Ohio 43210, and Beijing Nuclear Magnetic Resonance Center, Peking University, Beijing 100871, China

Received February 12, 2007; Revised Manuscript Received March 27, 2007

ABSTRACT: The conversion of prion protein (PrP) to the pathogenic PrP^{Sc} conformation is central to prion disease. Previous studies revealed that PrP interacts with lipids and the interaction induces PrP conformational changes, yet it remains unclear whether in the absence of any denaturing treatment, PrP−lipid interaction is sufficient to convert PrP to the classic proteinase K-resistant conformation. Using recombinant mouse PrP, we analyzed PrP−lipid interaction under physiological conditions and followed lipid-induced PrP conformational change with proteinase K (PK) digestion. We found that the PrP−lipid interaction was initiated by electrostatic contact and followed by hydrophobic interaction. The PrP−lipid interaction converted full-length α-helix-rich recombinant PrP to different forms. A significant portion of PrP gained a conformation reminiscent of PrP^{Sc}, with a PrP^{Sc}-like PK-resistant core and increased *β*-sheet content. The efficiency for lipid-induced PrP conversion depended on lipid headgroup structure and/or the arrangement of lipids on the surface of vesicles. When lipid vesicles were disrupted by Triton X-100, PrP aggregation was necessary to maintain the lipid-induced PrP^{Sc}-like conformation. However, the PK resistance of lipid-induced PrP^{Sc}-like conformation does not depend on amyloid fiber formation. Our results clearly revealed that the lipid interaction can overcome the energy barrier and convert full-length α-helix-rich PrP to a PrP^{Sc}-like conformation under physiological conditions, supporting the relevance of lipid-induced PrP conformational change to in vivo PrP conversion.

The conversion from the normal PrP^{C} conformation to the pathogenic PrP^{Sc} isoform is intimately associated with the pathogenesis of prion disease (*1*−*4*). PrP^{C} is tethered to lipid membranes through its glycosylphosphatidylinositol (GPI)[1] anchor. The discovery of two-dimensional arrays of PrP^{Sc} (*5*) led to the postulation that lipid membrane may contribute to the formation or stabilization of PrP^{Sc} during prion disease (*2*). This notion is supported by many experimental observations. Early studies revealed that, once PrP^{C} is converted to PrP^{Sc}, phosphatidylinositol phopholipase C cannot release it from lipid membranes (*6*, *7*), indicating that PrP^{Sc} binds to lipid membrane in a manner independent of its GPI anchor. Results from the cell-free conversion assay suggest that a GPI anchor-independent binding to lipid membranes is required for a successful PrP conversion (*8*). In prion-infected cells, changing lipid contents significantly alters the level of PrP^{Sc} (*9*, *10*). Re-incorporation of highly purified "prion rod" into liposomes results in higher prion infectivity (*11*). Similarly, the membrane-associated PrP^{Sc} infects cultured cells with higher efficiency than detergent-purified PrP^{Sc} (*12*). These results suggest the importance of a GPI anchor-independent lipid interaction in PrP conversion.

The GPI anchor-independent PrP−lipid binding has been investigated previously in several studies (*13*−*17*). A recent report showed that the anionic lipid bicelles with a 65 °C heating step converted α-helix-rich recombinant PrP to a *β*-sheet conformation (*17*). Addition of nonionic detergent to PrP and lipid bicelle mixtures induced amyloid fiber formation, and PrP in the amyloid fibrillar state has a PK-resistant core similar to PrP^{Sc}. This study clearly revealed a profound effect of anionic lipids on PrP conformation, yet the requirement of the 65 °C heating step for PrP conversion leaves the physiological relevance uncertain. Interestingly, similar partial denaturing treatments are generally required to convert α-helix-rich PrP to a *β*-sheet amyloidogenic conformation (*18*, *19*), presumably due to the energy barrier between the two conformational states (*20*).

Since PrP^{Sc} forms in vivo under physiological conditions, some cellular factors have to alleviate the energy barrier and facilitate PrP conversion. Recent advances in membrane protein folding field revealed that the interfacial region of lipid membranes has a potent ability to induce protein secondary structures (*21*, *22*), which suggest to us that the appropriate lipid compositions should be able to overcome the energy barrier and facilitate PrP conversion under physiological conditions.

The PrP−lipid interaction under native conditions has been studied using mainly biophysical methods. One study showed that, upon binding to lipid vesicles, the N-terminal unstruc-

† This work was supported by grants to J.M. from the Ellison Medical Foundation and American Federation in Aging Research.

* To whom correspondence should be addressed. Telephone: (614) 688-0408. Fax: (614) 292-4118. E-mail: ma.131@osu.edu.

‡ The Ohio State University.

§ Peking University.

[1] Abbreviations: PrP, prion protein; PK, proteinase K; GPI, glycosylphosphatidylinositol; rPrP, recombinant mouse PrP(23−230); CD, circular dichroism.

10.1021/bi700299h CCC: $37.00
Published on Web 05/16/2007

tured part of PrP becomes partially ordered while the C-terminal structured region is destabilized (*13*). A PrP fragment {residues 90−231 [PrP(90−231)]} was found to interact with a variety of lipid vesicles, resulting in secondary structure changes (*14*−*16*). These results reveal that the interaction with lipid membranes is capable of altering PrP conformation under native conditions. In particular, the interaction with anionic lipids induces the α-helix-rich recombinant PrP(90−231) to gain β-sheet content, which is similar to the PrP conformational change during prion disease (*23*−*26*). Besides the increase in β-sheet content, PrP^{Sc} is characterized by its C-terminal PK resistance, which is a more widely used and more stringent standard for the PrP^{Sc} conformation (*1*−*4*). However, it remains unclear whether the lipid interaction under native conditions is sufficient to induce an altered PrP conformation with the PrP^{Sc}-like PK resistance pattern.

Recombinant PrP used in studies described above differs from mammalian cell-expressed PrP^{C} in lacking N-linked glycosylation and the GPI anchor. Despite these differences, the relevance of recombinant PrP conversion to PrP conformational change in prion disease has been well supported. For example, amyloid fibers formed by recombinant PrP-(89−230) induced prion disease in transgenic mice overexpressing a similar PrP fragment (*27*, *28*). Expression of PrP without the GPI anchor in transgenic mice supported PrP conversion and the propagation of prion infectivity (*29*). Notably, the transgene PrP in these mice is very similar to recombinant PrP, without the GPI anchor and mostly unglycosylated (*29*). In addition, the seeding ability and morphology of recombinant PrP(23−144) amyloid fiber provide an explanation for the peculiar prion strains and species barrier (*30*, *31*). These findings suggest that the investigation of recombinant PrP conformational change will provide us with insights into the pathogenic PrP conversion in prion disease.

In this study, we used full-length recombinant mouse PrP-(23−230) to investigate whether PrP−lipid interaction can induce a PrP conformation with the classic PK-resistant pattern under physiological conditions. The answer to this question is crucial for the relevance of lipid-induced PrP conformational change to prion pathogenesis. We followed the lipid-induced PrP conversion with PK digestion and found that certain lipid compositions indeed converted α-helix-rich PrP to a PrP^{Sc}-like conformation with the characteristic PK-resistant pattern. The fact that lipid-induced PrP conversion occurs under an environment reminiscent of physiological condition supports the relevance of previously reported PrP−lipid interaction (*13*−*17*) to the pathogenesis of prion disease.

MATERIALS AND METHODS

Plasmid Construction, Recombinant PrP Expression, and Purification. The coding sequence of mouse PrP(23−230) was amplified by PCR and cloned into pPROEX-HTb (Invitrogen) or pET-28a(+) (Novagen) vectors in frame behind a linker sequence encoding six histidines followed by a tobacco etch virus protease or a thrombin cleavage site, respectively. One extra amino acid, glycine, or three amino acids, Gly-Ser-His, remained at the N-terminus after tobacco etch virus protease or thrombin cleavage of the linker, respectively. Recombinant mouse PrP(23−230) protein (rPrP) was purified as previously described (*32*). Protein concentrations used in our experiments were $OD_{280} = 0.25-0.36$, reflecting different batches of purifications. The molar concentrations were calculated using the ϵ_{280} molar extinction coefficient of 63,370 for mouse PrP(23−230) according to the ExPASy Proteomics Server of the Swiss Institute of Bioinformatics.

Preparation of Lipid Vesicles. Isolation of lipids from N2A cells or mouse brains was described previously (*33*). Other lipids were purchased from Avanti Polar Lipids, Inc. For vesicle preparation, lipids in chloroform were dried under a stream of nitrogen at 42 °C and then hydrated in 20 mM Tris-HCl buffer (pH 7.4) to reach a final concentration of 2.5 mg/mL unless indicated. Hydrated lipids were vortexed and sonicated in a cup-hold sonicator (Misonix Inc., model XL2020) until clear. The lipid vesicles were kept under argon.

Gradient Assays. For the discontinuous density gradient floatation assay, rPrP and lipid vesicles were mixed together for 5 min and applied to the high-density phase of the iodixanol density gradient as previously described (*33*). For the sucrose density gradient, samples were loaded atop the discontinuous sucrose gradient as previously described (*34*).

PrP Lipid Incubation and PK Digestion. Only soluble rPrP after a 1 h 100000*g* centrifugation was used for analyses. For rPrP and lipid incubation, 300 μL of rPrP ($OD_{280} = 0.25-0.36$) was mixed with 100 μL of lipid vesicles (lipid concentration of 2.5 mg/mL except were indicated). PrP and lipid mixtures were flushed with argon and incubated at 37 °C. For agitation with Triton X-100 treatment, the rPrP and lipid mixtures were incubated at 37 °C for the indicated times. After the incubation, 0.5% Triton X-100 was added and the mixture was agitated at 37 °C in an Eppendorf thermal mixer at 800 rpm. For PK digestion, 10 μL samples were removed and incubated with PK at 37 °C for 30 min with the indicated PK:rPrP molar ratios. The reaction was stopped by adding 5 mM phenylmethanesulfonyl fluoride (PMSF) and keeping the mixture on ice for 10 min. One-tenth of PK-digested samples were subject to SDS−PAGE and immunoblot analyses.

CD Spectroscopy. The far-UV CD spectra were obtained using a JOBIN YVON spectropolarimeter at 37 °C with an integration time of 1 s and a resolution of 0.5 nm. Five scans were averaged for each spectrum. The corresponding backgrounds (buffer with lipid at corresponding concentrations) were subtracted from the final spectra. No meaningful spectrum could be obtained below 195 nm due to low signal-to-noise ratio.

Transmission Electron Microscopy. Twenty microliters of each sample was mixed with 2% glutaraldehyde and kept at room temperature for 5 min. Copper precoated EM grids (Electron Microscopy Sciences) were layered on top of the sample drops for 5 min. The sample-containing grids were washed with distilled water, followed by staining with one drop of uranyl acetate (20 mg/mL) for 2 min at room temperature. Samples were analyzed on a Philips CM12 transmission electron microscopy at 80 kV with various magnifications.

RESULTS

Binding of rPrP to Lipids Involves both Electrostatic and Hydrophobic Interactions. We reported that full-length

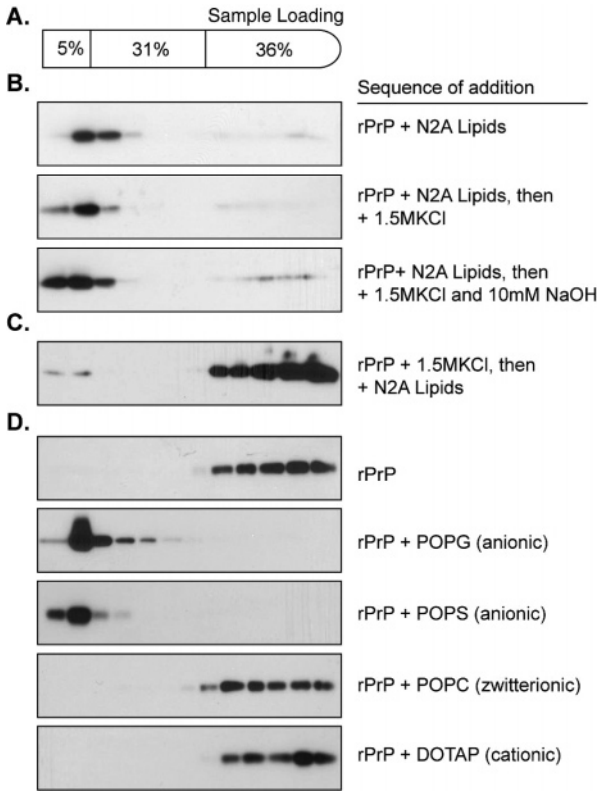

FIGURE 1: Interactions between rPrP and lipid vesicles. (A) The iodixanol density gradient. (B) rPrP was mixed with lipids isolated from N2A cells, with or without 1.5 M KCl or 1.5 MKCl and 10 mM NaOH extraction. (C) rPrP was first equilibrated with 1.5 M KCl and then mixed with N2A lipids with KCl the concentration maintained at 1.5 M. (D) rPrP was mixed with lipid vesicles composed of 2.5 mg/mL POPG, POPS, POPC, or DOTAP. PrP was detected by immunoblot analysis with the POM1 monoclonal antibody (*52*).

recombinant mouse PrP(23−230) (rPrP) bound to total lipids isolated from mouse brain in a previous study (*33*). To determine whether rPrP binds to lipids isolated from other sources, we monitored the binding of rPrP to total lipids isolated from cultured N2A cells (N2A lipids). Using the iodixanol density gradient (Figure 1A) (*33*), we found that rPrP bound to N2A lipids and migrated to the top of the gradient (Figure 1B). The binding resisted disruptions with high salt concentration and/or high pH, indicating a hydrophobic interaction. Interestingly, when rPrP was first equilibrated with 1.5 M KCl and then allowed to mix with N2A lipids, the binding was largely eliminated (Figure 1C).

Previous spectroscopic results suggested that the PrP−lipid interaction involves a binding step followed by its insertion into lipid bilayer (*14*). Therefore, the dramatic inhibitory effect observed here (Figure 1C) suggested to us that an initial electrostatic contact is likely involved in the early binding step, which was disrupted by the presence of 1.5 M KCl. This possibility was tested using individual phospholipids carrying different charges (Figure 1D and Table 1). We used phospholipids with palmitoyl and oleoyl chains because phospholipids with a monounsaturated fatty acyl chain have lower phase transition temperatures and are much more resistant to lipid peroxidation than polyunsaturated fatty acyl chains. Under our experimental condition, almost 100% of rPrP bound to anionic POPG or POPS. In contrast, there was no binding of rPrP to zwitterionic POPC or cationic DOTAP (Figure 1D). These results support the possibility that the PrP−lipid interaction is initiated by electrostatic contacts.

Table 1: Lipids Used in This Study

POPG	1-palmitoyl-2-oleoylphosphatidylglycerol
POPS	1-palmitoyl-2-oleoylphosphatidylserine
POPC	1-palmitoyl-2-oleoylphosphatidylcholine
POPA	1-palmitoyl-2-oleoylphosphatidic acid
DOTAP	1,2-dioleoyl-3-trimethylammonium propane
brain sulfatide	HSO_4-3-Galβ1−1′ceramid

Interaction with Lipid Induces a Conformational Change in rPrP. To ensure that our experimental system recapitulated the reported biophysical characteristics of PrP−lipid interaction under native conditions (*14*, *15*), we monitored the influence of lipid interaction on rPrP conformation by far-UV circular dichroism (CD). The spectrum of rPrP alone is consistent with a conformation enriched with α-helices (Figure 2A) (*35*), which was further verified by the two-dimensional $^1H-^{15}N$ NMR spectrum showing that its overall fold was predominantly α-helices (Figure S1 of the Supporting Information). After incubation with POPG at 37 °C for 1 h (Figure 2A), the CD spectrum of rPrP showed an increase in negative ellipticity with a minimum peak around 216 nm, suggesting an increase in β-sheet content. These results are consistent with previous reports (*14*, *15*).

After establishing the system, we first tested the effect of longer incubation with lipid vesicles on PrP conformation. We found that a 24 or 48 h incubation of rPrP with POPG at 37 °C resulted in additional changes in CD spectra (Figure 2A), which may suggest further conformational alterations. As a control, rPrP was incubated with zwitterionic POPC, and no conformational change was detected even after a prolonged incubation (Figure S2 of the Supporting Information). To determine whether the increase in the β-sheet content of rPrP is accompanied by increased PK resistance, PK digestion was performed with PK:rPrP molar ratios of 1:16, 1:7.5, and 1:3. Two PK-resistant bands around 15 and 14.5 kDa were detected after a 24 h incubation with POPG (Figure 2C), whereas rPrP incubated with either buffer alone or POPC remained PK sensitive. Interestingly, the interaction with POPG also dramatically stabilized rPrP at 37 °C (Figure 2C, compare samples without PK digestion).

To determine the effect of salt, 150 mM NaCl was added to the reaction mixture. We observed further changes in the CD spectra (Figure 2B). Interestingly, addition of 150 mM NaCl significantly enhanced the efficiency for PK-resistant rPrP formation (Figure 2D). A single 15 kDa PK-resistant band was clearly detectable after incubation for merely 1 h. The amount of PK-resistant rPrP is similar to the undigested control sample loaded on SDS−PAGE (Figure 2D, −PK). Since rPrP in the undigested control sample was 10% of that used in PK digestion, we estimated that around 10% of lipid-interacting rPrP gained PK resistance despite an almost 100% binding of rPrP to anionic POPG (Figure 1D). Digestion of lipid-interacting rPrP with increased amounts of PK revealed that the lipid-induced rPrP conformation has a remarkably high PK resistance (Figure 2E), and the PK-resistant band was clearly detectable after a 30 min digestion at 37 °C with the PK:rPrP molar ratio as high as 150:1 (equal to 3.75 mg/mL PK). In contrast, rPrP remained PK-sensitive after incubation with either salt alone or salt and POPC (Figure

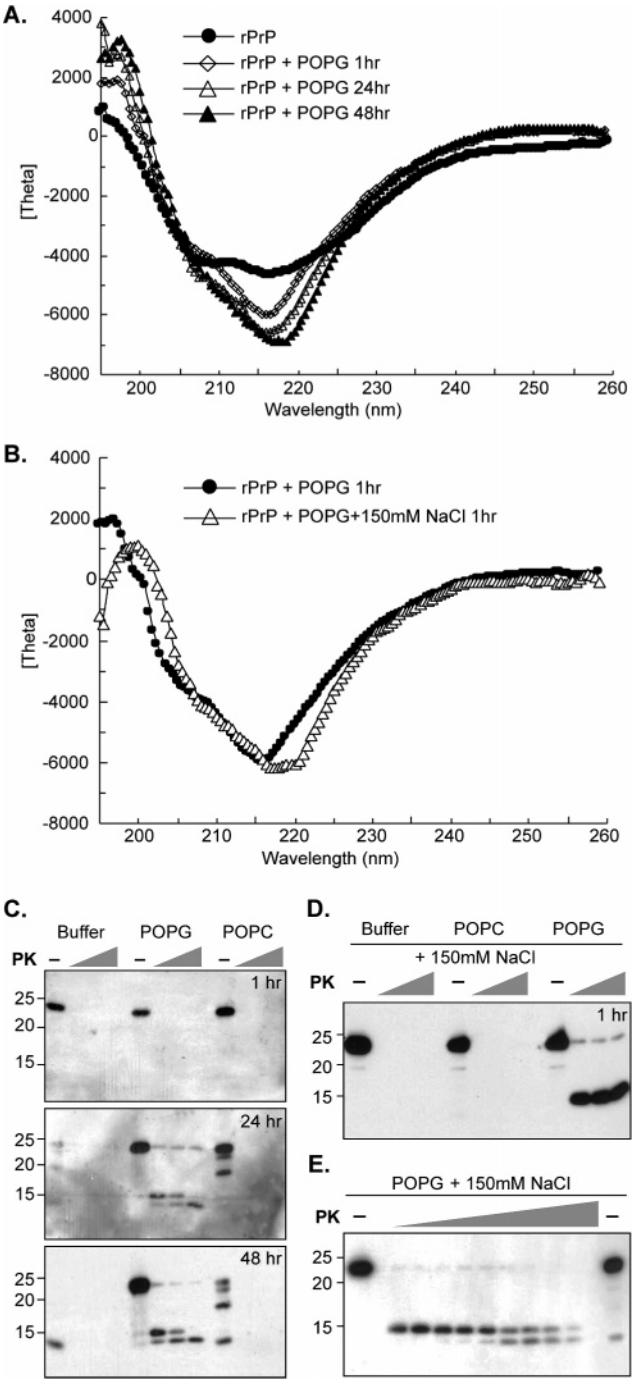

FIGURE 2: Anionic lipid interaction induced a conformational change in rPrP. (A) Far-UV CD spectra for rPrP or rPrP incubated with POPG for the indicated time. The unit of θ is degrees cm^{-1} mol^{-1} L. (B) Same as panel A except 150 mM NaCl was added. (C) PK digestion of rPrP after incubation at 37 °C for the indicated time with buffer, POPG, or POPC. The PK:rPrP molar ratios were 1:16, 1:7.5, and 1:3. (D) Same as panel C except 150 mM NaCl was added. (E) rPrP was incubated with POPG vesicles for 1 h at 37 °C in the presence of 150 mM NaCl and then subjected to PK digestion with PK:rPrP molar ratios of 1:16, 1:7.5, 1:3, 1:1.5, 3:1, 15:1, 30:1, 75:1, 150:1, and 300:1. PrP was detected by immunoblot analysis with the POM1 antibody.

2D), indicating that the anionic POPG−rPrP interaction is the major determinant of rPrP conformational change.

Both Charge and Lipid Headgroup Structure Influence rPrP Conformational Change. The requirement for the anionic POPG led us to ask whether the negative charges on lipid vesicles are important for rPrP conversion. Using

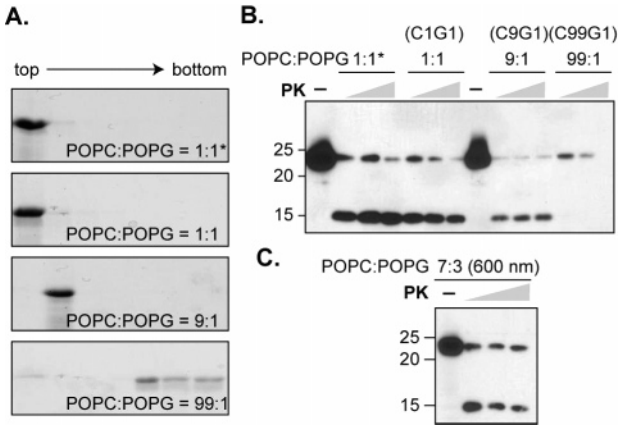

FIGURE 3: Negative charges on lipid vesicles affect rPrP binding and conformational change. (A) rPrP was mixed with lipid vesicles composed of POPC and POPG at the indicated ratios. The concentration of total lipids was 2.5 mg/mL, except for the top panel (1:1*) where it was 5 mg/mL. The presence of rPrP was detected by Coomassie blue staining. (B) PK digestion of rPrP incubated at 37 °C with indicated lipid vesicles in the presence of 150 mM NaCl for 1 h. (C) PK digestion of rPrP incubated with 600 nm diameter liposomes composed of POPC and POPG at a 7:3 molar ratio. The incubation was carried out at 37 °C for 24 h in the presence of 150 mM NaCl. The PK:rPrP molar ratios were 1:16, 1:7.5, and 1:3 for both panels B and C, and PrP was detected by immunoblot analysis with the POM1 antibody.

zwitterionic POPC mixing with decreasing amounts of POPG, we observed a reduced binding of rPrP to lipid vesicles (Figure 3A). When the POPC:POPG ratio was at 9:1 (designated as C9G1), the majority of rPrP remained lipid-bound and migrated to the top of the gradient. The appearance of rPrP in the second fraction (Figure 3A) is likely due to the aggregation of rPrP-bound lipid vesicles since visible aggregates were observed under this condition. When the POPC:POPG ratio reached 99:1 (C99G1), the majority of rPrP remained in the bottom fractions of the gradient (Figure 3A), indicating that they were not lipid-bound. Similarly, the intensity of the 15 kDa PK-resistant band decreased with reduced POPG content (Figure 3B), suggesting that the rPrP conformational change was closely associated with its interaction with anionic POPG.

The morphology of lipid vesicles was monitored by freeze fracture electron microscopy. As expected from lipid vesicles prepared by sonication, POPC and C9G1 formed small liposomes (Figure S3 of the Supporting Information). Fewer lipid vesicles were observed with anionic POPG, presumably due to the repulsion by its negative charge resulting in micelle formation instead of liposome. These results suggested that the charge-dependent lipid binding and conformational change of rPrP appeared to be independent of the shape of lipid vesicles. This conclusion was further supported by preparing large unilamellar vesicles (7:3 POPC:POPG, 600 nm in diameter) by extrusion, which induced the similar 15 kDa PK-resistant rPrP band (Figure 3C).

Next, we asked whether rPrP conformational change is solely governed by negative charges or by both negative charge and lipid structure. Under the same condition, much less PK-resistant rPrP was detected after incubation with anionic POPS (Figure 4A). However, when the same amount of POPS was simply mixed with zwitterionic POPC at a 1:1 ratio, the conversion of rPrP to the PK-resistant conformation was at least as efficient as with POPG. Under our experi-

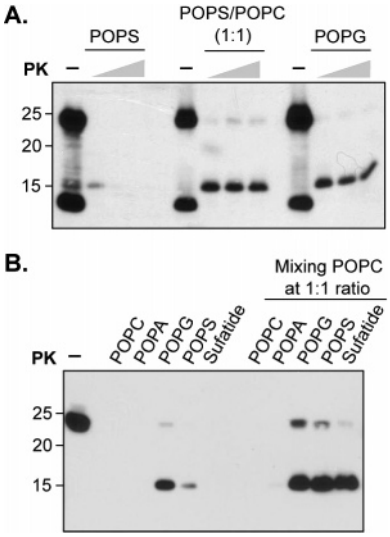

FIGURE 4: Different lipid compositions affect rPrP conformation. (A) rPrP was incubated with POPS (2.5 mg/mL), POPS and POPC (5 mg/mL), or POPG (2.5 mg/mL) and subjected to PK digestion with PK:rPrP molar ratios of 1:16, 1:7.5, and 1:3. (B) rPrP was incubated with various lipids as indicated with the total lipid concentration kept at 2.5 mg/mL before mixing with rPrP, and subjected to PK digestion with a PK:rPrP molar ratio of 1:16. PrP was detected by immunoblot analysis with the POM1 antibody.

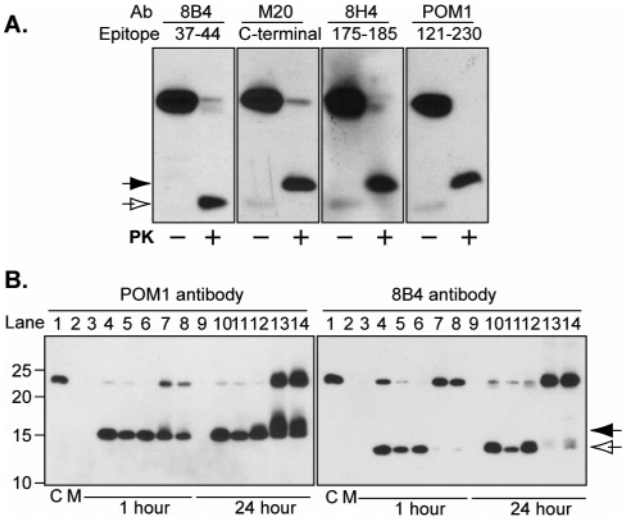

FIGURE 5: Characterizing the PK-resistant PrP conformation. (A) rPrP was incubated with C9G1 vesicles and subjected to PK digestion with PK:rPrP molar ratios of 1:7.5. Antibodies recognizing the indicated epitopes were used to detect the PK-resistant PrP fragment. (B) Lane 1 contained undigested PrP and lane 2 protein standards. Lanes 3−8 contained PrP incubated with different lipids for 1 h and subjected to PK digestion with a PK:PrP molar ratio of 1:16. The following lipids were used: POPC (lane 3), POPG (lane 4), C9G1 (lane 5), POPS and POPC (lane 6), N2A lipids (lane 7), and mouse brain lipids (lane 8). Lanes 9−14 were the same as lanes 3−8 but with a 24 h incubation. PrP was detected by immunoblot analyses with the POM1 or 8B4 antibody as indicated.

mental condition, the binding of rPrP to either POPS or POPG was almost 100% (Figure 1D). In addition, the fatty acyl chains were exactly the same between POPS and POPG. Therefore, these results indicated that the structure of the lipid headgroup affects the resulting rPrP conformation. This notion was further supported by using anionic POPA and brain-enriched glycolipid, sulfatide (3′-sulfogalactosylceramide) (Table 1). Although rPrP bound to both anionic lipids similar to its binding to POPG (data not shown), no PK-resistant rPrP was detected after incubation with either POPA or sulfatide alone (Figure 4B). However, when mixed with zwitterionic POPC at a 1:1 ratio, a strong PK-resistant PrP band was observed with sulfatide, POPG, and POPS, but very little with the POPA/POPC mixture. Collectively, these results indicated that the conversion of rPrP to the PK-resistant conformation depended on the negative charges of lipid vesicles as well as the structure and/or the arrangement of lipid headgroups.

The 15 kDa PK-Resistant Fragment Is the C-Terminal rPrP Fragment. PrP^{Sc} has a highly PK-resistant C-terminal fragment, while its N-terminus remains PK-sensitive (*1*). The specific C-terminal PK resistance differentiates between nonspecific PrP aggregation and the PrP^{Sc} conformation. To determine whether the 15 kDa PK-resistant rPrP band was at the C-terminus, we probed it with a panel of antibodies. All the antibodies recognizing C-terminal epitopes of PrP detected the 15 kDa band (Figure 5A, solid arrow), which was not recognized by the N-terminal epitope-specific 8B4 antibody (*36*, *37*), indicating that the 15 kDa band is similar to the PK-resistant core of PrP^{Sc}.

Surprisingly, the 8B4 antibody detected an additional PK-resistant band around 13.5 kDa, which was not recognized by any of other antibodies (Figure 5A, empty arrow). This puzzling observation raised the question of whether the N-terminal PK-resistant conformation was also induced by other lipid compositions. We incubated rPrP with various lipid combinations for 1 (Figure 5B, lanes 3−8) or 24 h (Figure 5B, lanes 9−14) and detected the PK-resistant PrP fragments with either POM1 or 8B4 antibody. While the levels of C-terminal 15 kDa resistant fragment remained relatively similar, very little N-terminal resistant fragment was detected with mixed lipids isolated from N2A cells or mouse brains (Figure 5B, lanes 6, 7, 13, and 14 for POM1 and 8B4), indicating that the two PK-resistant fragments were not always associated with each other.

Aggregation of PrP Stabilizes the Lipid-Induced PK-Resistant PrP Conformation. Disrupting lipid vesicles with 0.5% Triton X-100 completely abolished the PK resistance of rPrP (Figure 6A), which suggested that the binding of rPrP to lipid vesicles might be required for the stability of the altered rPrP conformation. Disrupting lipid vesicles would render them PK-sensitive. Since authentic PrP^{Sc} is highly aggregated, we hypothesized that the aggregation of rPrP molecules may stabilize the lipid-induced PK-resistant conformation when lipid vesicles are disrupted.

To increase the likelihood that rPrP would aggregate, the lipid rPrP mixtures were agitated at 37 °C for 16 h in the presence of Triton X-100. The aggregation status of rPrP was monitored by a sucrose gradient analysis (*34*). In this gradient, the majority of the monomeric rPrP remained at the top, even after a 16 h agitation in the presence of Triton X-100 (Figure 6B, top and second panel). After binding to POPG vesicles, rPrP spread at the middle and bottom fractions of the gradient, likely due to the migration of POPG vesicles in the gradient. When Triton X-100 was included, the majority of rPrP appeared at the bottom of the gradient (Figure 6B, bottom panel), indicating the disruption of POPG vesicles and aggregation of rPrP. The reappearance of a small amount of rPrP in the top fractions supported a thorough detergent extraction.

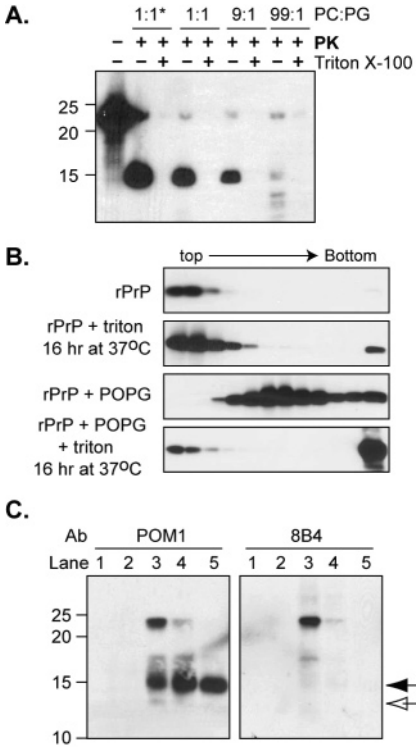

FIGURE 6: Aggregation stabilizing the PK-resistant rPrP conformation. (A) rPrP was mixed with POPC and POPG in the presence of 150 mM NaCl and incubated at 37 °C for 1 h. PK digestion was carried out with a PK:rPrP molar ratio of 1:16 in the presence or absence of 0.5% Triton X-100. PrP was detected by immunoblot analysis with the polyclonal M20 antibody. (B) rPrP with indicated treatments was loaded on top of the sucrose gradient, and the presence of rPrP was detected with immunoblot analysis with the POM1 antibody. For panels with Triton X-100 treatment, rPrP and lipid mixtures were incubated at 37 °C for 1 h. Then, 0.5% Triton X-100 (final concentration) was added and agitated at 37 °C for 16 h. (C) rPrP was incubated with buffer (lane 1), POPC (lane 2), POPG (lane 3), POPC and POPG at a 1:1 ratio (lane 4), and C9G1 (lane 5) for 1 h at 37 °C in the presence of 150 mM NaCl. After incubation, 0.5% Triton X-100 (final concentration) was added and samples were agitated for 16 h at 37 °C at 800 rpm. PK digestion was performed with a PK:rPrP ratio of 1:16. PrP was detected by immunoblot analyses with POM1 and 8B4 antibodies.

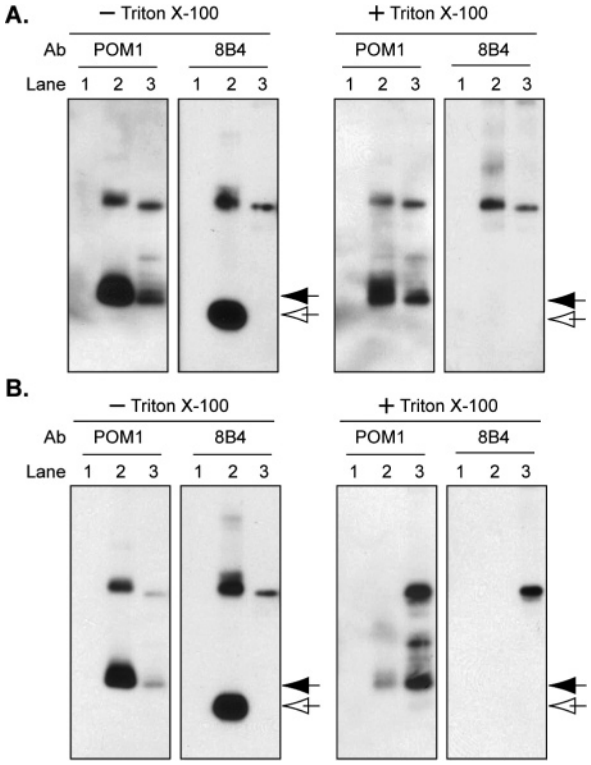

FIGURE 7: PK-resistant rPrP conformation that formed with a lower lipid:rPrP ratio. Recombinant PrP was incubated with POPC (lane 1), POPG (lane 2), or POPG10% (lane 3) for 6 days at 37 °C in the presence of 150 mM NaCl. (A) After incubation, samples were agitated at 800 rpm for 16 h in the presence or absence of 0.5% Triton X-100. PK digestion was carried out at 37 °C for 30 min with a PK:rPrP molar ratio of 1:16. PrP was detected with the POM1 or 8B4 antibody as indicated. (B) Same as panel A except samples were incubated without agitation.

To determine whether PK resistance remained in aggregated rPrP molecules, rPrP was incubated with various lipid combinations followed by agitation in the presence of Triton X-100 and then subjected to PK digestion. The PK:rPrP molar ratio was 1:16, which was much higher than the regular ratio of 1:50. In control samples incubated in buffer alone or with POPC (Figure 6C, lanes 1 and 2), rPrP remained PK-sensitive. However, in samples incubated with lipid combinations that were able to induce the PK-resistant rPrP, the 15 kDa C-terminal fragment was detected (Figure 6C, POM1, lanes 3−5), while the N-terminal PK-resistant fragment was not (Figure 6C, 8B4). Together, these results indicated that the aggregation of rPrP molecules is able to stabilize the anionic lipid-induced PrP^{Sc}-like conformation.

An alternative approach is to decrease the lipid:rPrP ratio, which will improve the opportunity for rPrP molecules to interact with each other on the surface of lipid vesicles and, thereby, stabilize the anionic lipid-induced PK-resistant conformation. To test this possibility, we decreased the amount of POPG to 10% of the amount used in previous analyses (designated as POPG10%). As controls, rPrP/POPC and rPrP/POPG mixtures were subjected to the same treatment.

All rPrP/lipid mixtures were incubated at 37 °C for 6 days. After the incubation, part of the mixtures was agitated for an additional 16 h at 37 °C in the presence or absence of Triton X-100 (Figure 7A). Without Triton, a weaker 15 kDa PK-resistant rPrP band was detected with POPG10% (Figure 7A, −Triton X-100, POM1; compare lanes 2 and 3), which is consistent with the notion that the rPrP conformational change is dependent on the amount of anionic lipids. Interestingly, the N-terminal PK-resistant band was not detected in rPrP incubated with POPG10% (Figure 7A, −Triton X-100, 8B4), suggesting that its appearance requires a higher POPG:rPrP ratio. In the presence of Triton (Figure 7A, +Triton X-100), only the 15 kDa C-terminal PK-resistant fragment was detected, supporting the possibility that the aggregation of rPrP molecules stabilized the PK-resistant conformation with the C-terminal resistant fragment.

Another part of the mixture was incubated at 37 °C for an additional 16 h but without agitation. Without Triton, the result was similar to that described above, more PK-resistant rPrP with POPG and no N-terminal resistant band with POPG10% (Figure 7B, −Triton X-100). However, in samples incubated with Triton, more PK-resistant rPrP was detected in rPrP incubated with POPG10% (Figure 7B, +Triton X-100, POM1; compare lanes 2 and 3). This result indicated that a lower lipid:rPrP ratio increased the level of rPrP aggregation on the surface of lipid vesicles, which stabilized

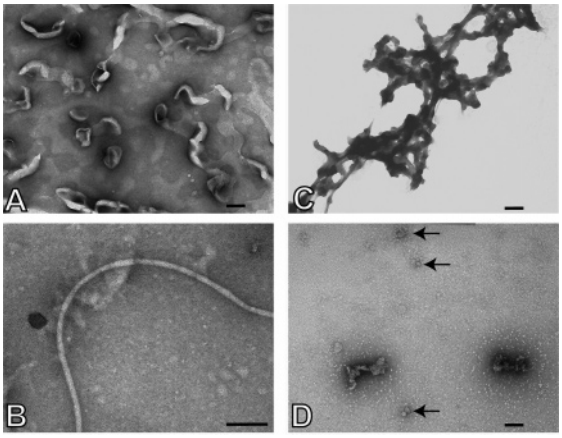

FIGURE 8: Morphology of rPrP aggregates. (A) Recombinant PrP was incubated with POPG at 37 °C for 24 h in the presence of 150 mM NaCl. (B) Recombinant PrP incubated with POPG10% (the POPG concentration before mixing with rPrP was 0.25 mg/mL) at 37 °C for 1 month in the presence of 150 mM NaCl. (C) Recombinant PrP was incubated with C9G1 at 37 °C for 17 days in the presence of 150 mM NaCl. (D) The PrP/C9G1 mixture from panel C was agitated for 16 h in the presence of 0.5% Triton X-100. Arrows point to smaller aggregates. The bar corresponds to 50 nm.

the PK-resistant conformation even when lipid vesicles were disrupted by Triton X-100. In all these manipulations, the rPrP incubated with zwitterionic POPC remained PK-sensitive (lane 1 in all panels of Figure 7A,B), supporting the requirement of anionic lipid interaction for rPrP conversion. Together, these results suggested that the anionic lipid-induced PrP^{Sc}-like rPrP conformation, but not the N-terminal PK-resistant rPrP form, can be stabilized by the aggregation of rPrP molecules.

Lipid-Induced PK Resistance of rPrP Does Not Correlate with Fiber Formation. Electron microscopic (EM) analysis was performed to monitor the morphology of rPrP incubated under various conditions (Figure 8). In the presence of 150 mM NaCl, rPrP incubated with POPG formed a "wormlike" structure with a diameter of ~40−50 nm (Figure 8A), which were not observed in control samples containing POPG alone or rPrP with POPC (data not shown). However, these wormlike structures did not grow into amyloid fibers even after a very long period of incubation (data not shown). Rarely, amyloid fiber-like structures with a width of ~10 nm could be found with samples incubated with POPG10% (Figure 8B). When rPrP was incubated with C9G1 vesicles, large network-like structures were observed (Figure 8C). After agitation in the presence of Triton X-100, the large network-like structures disappeared and only amorphous aggregates were observed (Figure 8D). Since PK-resistant rPrP was detected under all these conditions, these results suggested that amyloid fiber formation was not required for the anionic lipid-induced PK-resistant rPrP conformation.

DISCUSSION

Consistent with previous reports (*13*−*17*), we showed that rPrP interacts with anionic lipids and the interaction increased the β-sheet content of rPrP. In addition, our study also revealed that, under physiological conditions, the binding of rPrP to certain anionic lipid vesicles is sufficient to convert a significant portion of α-helix-rich rPrP to a conformation similar to PrP^{Sc}, which has the characteristic PK-resistant pattern. The amount of negative charges and the lipid headgroup structure of lipid vesicles significantly affect the resulting rPrP conformation. When lipid vesicles are disrupted by detergent, PrP aggregation is necessary to maintain the anionic lipid-induced PK-resistant conformation. Our findings support both the physiological relevance of previously reported lipid-induced PrP conformational change (*13*−*17*) and the proposition that lipid membranes may provide a support for the PrP^{Sc} conformation (*2*, *38*).

Using lipid bicelles, Luhrs et al. (*17*) showed that a 65 °C heating step was required in their system for rPrP conformational change. In our system, the lipid-induced PrP^{Sc}-like conformation was formed under physiological conditions. This difference is likely due to the difference in lipid vesicles used in two studies. The lipid bicelles used in their study differ in both composition and shape from lipid vesicles used in our study, which may result in a different presentation of lipid headgroups. Nevertheless, both our studies support a significant influence of anionic lipid membranes on rPrP conformation, which may contribute to PrP conversion as previously proposed (*2*, *38*).

An interesting finding in our study is that the lipid-induced PrP^{Sc}-like conformation does not correlate to amyloid fiber formation. Previous reports of full-length rPrP conversion are all associated with the generation of amyloid fibers, which are formed after denaturant treatment (*19*), denaturant treatment with a heating step (*39*), or lipid bicelles with a 65 °C heating step (*17*). Since full-length PrP^{Sc} isolated from diseased brain is not in an amyloid fiber state (*40*, *41*) and the most infectious prion protein particles are PrP oligomers instead of amyloid fibers (*42*), the non-amyloid-associated PrP^{Sc}-like conformation identified in this study may recapitulate certain characteristics of PrP^{Sc}.

Another novel finding in our study is that the anionic lipid vesicles induce two rPrP forms with either the C-terminus or the N-terminus of rPrP being resistant to PK digestion. The appearance of both N- and C-terminal PK-resistant fragments after lipid binding is suspiciously similar to that of the transmembrane form of PrP (*43*). However, it is unlikely that the transmembrane PrP was formed in our system since neither signal sequences nor translocon was present. Generally, a protein cannot by itself penetrate across a lipid membrane. Although some protein toxins, such as diphtheria and anthrax toxin, are known to form proteinaceous channels and translocate part of the toxin across membrane (*44*), PrP is not known to have any of these characteristics. In addition, PK-resistant rPrP was efficiently formed after incubation with anionic POPG, which tends to form micelles without an interior aqueous core and would prohibit a transmembrane topology. Moreover, a transmembrane protein would have been protected from any amount of PK because the lipid bilayer is impermeable to PK. In contrast, the lipid-induced PK-resistant rPrP is susceptible to the digestion of a large amount of PK (Figure 2E). Furthermore, only the C-terminal PrP^{Sc}-like PK-resistant band remains after agitation in the presence of Triton X-100. Even for some unexplainable reasons that rPrP were still protected by lipid vesicles after Triton extraction, both N- and C-terminal PK-resistant bands should have been protected. These analyses suggest to us that the presence of two PK-resistant forms of rPrP is not due to the formation of

transmembrane PrP. Instead, a lipid-induced rPrP conformational change is a more plausible explanation.

The role of lipid in PrP conversion seems paradoxical to the observation that PrP was efficiently converted in the presence of detergent in a modified version of protein misfolding cyclic amplification (PMCA) (*45*) or in PMCA (*46*). However, detergent extraction may not completely remove lipid molecules from aggregated protein, which is supported by the presence of lipid molecules in highly purified prion rods (*47*). In addition, these in vitro PrP conversion assays are performed with brain homogenates and the presence of other polyanions like RNA and proteoglycan may substitute for the role of anionic lipid membranes (*48*, *49*). Furthermore, detergent itself is a bipolar molecule, which may replace the role of lipid to certain extent. It has been shown that anionic detergent sarkosyl induces PrP aggregation and fibril formation, but without the proper PK resistance (*50*). Low concentrations of SDS maintain a β-sheet-rich, transiently soluble state of PrP(27−30) (*51*). Thus, the presence of detergent in the in vitro PrP conversion assays does not necessary rule out the involvement of lipid membrane in PrP conversion in a biological system. On the contrary, the electrostatic interaction-initiated PrP−lipid contact is consistent with the observations that charged molecules like polyamines or sulfated molecules inhibit PrP^{Sc} production in cultured cells (*3*). In addition, the cell surface-localized anionic proteoglycans, the raft-localized gangliosides with bulky carbohydrate structures and terminal sialic acids, and the N-linked oligosaccharides on PrP would prevent PrP−lipid interaction, which would be consistent with the rarity of spontaneous PrP conversion.

The transgenic mouse experiment revealed that PrP without its GPI anchor still supports the conformation change and the propagation of prion infectivity (*29*), yet the generation of prion infectivity in these mice does not exclude the involvement of lipid membrane. Secreted anchorless PrP may interact with lipid membranes it normally would not encounter, which may be responsible for the massive accumulation of PK-resistant PrP around vascular endothelial cells (*29*). The authors of that study postulated a possible facilitating effect by lipid membrane-associated proteoglycans (*29*). It is also possible that the lipid membranes themselves play a role in this process.

Our study characterized how lipid converts α-helix-rich rPrP to a PrP^{Sc}-like conformation with an increased β-sheet content and a PK-resistant pattern similar to that of PrP^{Sc}. The fact that lipid-induced PrP conversion occurs under physiological conditions provides strong support for the relevance of lipid−PrP interaction to the pathogenic changes in prion disease. Further investigation of this process together with the relationship between lipid-induced PrP^{Sc}-like conformation and prion infectivity may help us to elucidate the pathogenic mechanism of prion disease.

ACKNOWLEDGMENT

We thank Drs. Adriano Aguzzi and Man-Sun Sy for providing antibodies and Kathy Wolken at the Ohio State University image facility for technique help.

SUPPORTING INFORMATION AVAILABLE

NMR spectra of rPrP (Figure S1), CD spectrum of rPrP incubated with POPC compared with that of rPrP alone (Figure S2), and images of freeze-fracture EM analysis of lipid vesicles (Figure S3). This material is available free of charge via the Internet at http://pubs.acs.org.

REFERENCES

1. Prusiner, S. B. (1998) Prions, *Proc. Natl. Acad. Sci. U.S.A. 95*, 13363−13383.
2. Caughey, B. (2003) Prion protein conversions: Insight into mechanisms, TSE transmission barriers and strains, *Br. Med. Bull. 66*, 109−120.
3. Weissmann, C., and Aguzzi, A. (2005) Approaches to therapy of prion diseases, *Annu. Rev. Med. 56*, 321−344.
4. Aguzzi, A. (2006) Prion diseases of humans and farm animals: Epidemiology, genetics, and pathogenesis, *J. Neurochem. 97*, 1726−1739.
5. Wille, H., Michelitsch, M. D., Guenebaut, V., Supattapone, S., Serban, A., Cohen, F. E., Agard, D. A., and Prusiner, S. B. (2002) Structural studies of the scrapie prion protein by electron crystallography, *Proc. Natl. Acad. Sci. U.S.A. 99*, 3563−3568.
6. Stahl, N., Borchelt, D. R., and Prusiner, S. B. (1990) Differential release of cellular and scrapie prion proteins from cellular membranes by phosphatidylinositol-specific phospholipase C, *Biochemistry 29*, 5405−5412.
7. Caughey, B., Neary, K., Buller, R., Ernst, D., Perry, L. L., Chesebro, B., and Race, R. E. (1990) Normal and scrapie-associated forms of prion protein differ in their sensitivities to phospholipase and proteases in intact neuroblastoma cells, *J. Virol. 64*, 1093−1101.
8. Baron, G. S., and Caughey, B. (2003) Effect of glycosylphosphatidylinositol anchor-dependent and -independent prion protein association with model raft membranes on conversion to the protease-resistant isoform, *J. Biol. Chem. 278*, 14883−14892.
9. Taraboulos, A., Scott, M., Semenov, A., Avrahami, D., Laszlo, L., and Prusiner, S. B. (1995) Cholesterol depletion and modification of COOH-terminal targeting sequence of the prion protein inhibit formation of the scrapie isoform, *J. Cell Biol. 129*, 121−132.
10. Naslavsky, N., Shmeeda, H., Friedlander, G., Yanai, A., Futerman, A. H., Barenholz, Y., and Taraboulos, A. (1999) Sphingolipid depletion increases formation of the scrapie prion protein in neuroblastoma cells infected with prions, *J. Biol. Chem. 274*, 20763−20771.
11. Gabizon, R., McKinley, M. P., and Prusiner, S. B. (1987) Purified prion proteins and scrapie infectivity copartition into liposomes, *Proc. Natl. Acad. Sci. U.S.A. 84*, 4017−4021.
12. Baron, G. S., Magalhaes, A. C., Prado, M. A., and Caughey, B. (2006) Mouse-adapted scrapie infection of SN56 cells: Greater efficiency with microsome-associated versus purified PrP-res, *J. Virol. 80*, 2106−2117.
13. Morillas, M., Swietnicki, W., Gambetti, P., and Surewicz, W. K. (1999) Membrane environment alters the conformational structure of the recombinant human prion protein, *J. Biol. Chem. 274*, 36859−36865.
14. Sanghera, N., and Pinheiro, T. J. (2002) Binding of prion protein to lipid membranes and implications for prion conversion, *J. Mol. Biol. 315*, 1241−1256.
15. Kazlauskaite, J., Sanghera, N., Sylvester, I., Venien-Bryan, C., and Pinheiro, T. J. (2003) Structural changes of the prion protein in lipid membranes leading to aggregation and fibrillization, *Biochemistry 42*, 3295−3304.
16. Critchley, P., Kazlauskaite, J., Eason, R., and Pinheiro, T. J. (2004) Binding of prion proteins to lipid membranes, *Biochem. Biophys. Res. Commun. 313*, 559−567.
17. Luhrs, T., Zahn, R., and Wuthrich, K. (2006) Amyloid formation by recombinant full-length prion proteins in phospholipid bicelle solutions, *J. Mol. Biol. 357*, 833−841.
18. Swietnicki, W., Morillas, M., Chen, S. G., Gambetti, P., and Surewicz, W. K. (2000) Aggregation and fibrillization of the recombinant human prion protein huPrP90−231, *Biochemistry 39*, 424−431.
19. Bocharova, O. V., Breydo, L., Parfenov, A. S., Salnikov, V. V., and Baskakov, I. V. (2005) In vitro conversion of full-length mammalian prion protein produces amyloid form with physical properties of PrP(Sc), *J. Mol. Biol. 346*, 645−659.
20. Baskakov, I. V., Legname, G., Prusiner, S. B., and Cohen, F. E. (2001) Folding of prion protein to its native α-helical conformation is under kinetic control, *J. Biol. Chem. 276*, 19687−19690.

21. White, S. H., and Wimley, W. C. (1999) Membrane protein folding and stability: Physical principles, *Annu. Rev. Biophys. Biomol. Struct. 28*, 319−365.
22. Wimley, W. C., Hristova, K., Ladokhin, A. S., Silvestro, L., Axelsen, P. H., and White, S. H. (1998) Folding of β-sheet membrane proteins: A hydrophobic hexapeptide model, *J. Mol. Biol. 277*, 1091−1110.
23. Caughey, B. W., Dong, A., Bhat, K. S., Ernst, D., Hayes, S. F., and Caughey, W. S. (1991) Secondary structure analysis of the scrapie-associated protein PrP 27−30 in water by infrared spectroscopy, *Biochemistry 30*, 7672−7680.
24. Caughey, B., Raymond, G. J., and Bessen, R. A. (1998) Strain-dependent differences in β-sheet conformations of abnormal prion protein, *J. Biol. Chem. 273*, 32230−32235.
25. Pan, K. M., Baldwin, M., Nguyen, J., Gasset, M., Serban, A., Groth, D., Mehlhorn, I., Huang, Z., Fletterick, R. J., Cohen, F. E., et al. (1993) Conversion of α-helices into β-sheets features in the formation of the scrapie prion proteins, *Proc. Natl. Acad. Sci. U.S.A. 90*, 10962−10966.
26. Safar, J., Roller, P. P., Gajdusek, D. C., and Gibbs, C. J., Jr. (1993) Thermal stability and conformational transitions of scrapie amyloid (prion) protein correlate with infectivity, *Protein Sci. 2*, 2206−2216.
27. Legname, G., Baskakov, I. V., Nguyen, H. O., Riesner, D., Cohen, F. E., DeArmond, S. J., and Prusiner, S. B. (2004) Synthetic mammalian prions, *Science 305*, 673−676.
28. Legname, G., Nguyen, H. O., Baskakov, I. V., Cohen, F. E., Dearmond, S. J., and Prusiner, S. B. (2005) Strain-specified characteristics of mouse synthetic prions, *Proc. Natl. Acad. Sci. U.S.A. 102*, 2168−2173.
29. Chesebro, B., Trifilo, M., Race, R., Meade-White, K., Teng, C., LaCasse, R., Raymond, L., Favara, C., Baron, G., Priola, S., Caughey, B., Masliah, E., and Oldstone, M. (2005) Anchorless prion protein results in infectious amyloid disease without clinical scrapie, *Science 308*, 1435−1439.
30. Vanik, D. L., Surewicz, K. A., and Surewicz, W. K. (2004) Molecular basis of barriers for interspecies transmissibility of mammalian prions, *Mol. Cell 14*, 139−145.
31. Jones, E. M., and Surewicz, W. K. (2005) Fibril conformation as the basis of species- and strain-dependent seeding specificity of mammalian prion amyloids, *Cell 121*, 63−72.
32. Zahn, R., von Schroetter, C., and Wuthrich, K. (1997) Human prion proteins expressed in *Escherichia coli* and purified by high-affinity column refolding, *FEBS Lett. 417*, 400−404.
33. Wang, X., Wang, F., Arterburn, L., Wollmann, R., and Ma, J. (2006) The interaction between cytoplasmic prion protein and the hydrophobic lipid core of membrane correlates with neurotoxicity, *J. Biol. Chem. 281*, 13559−13565.
34. Nazor, K. E., Kuhn, F., Seward, T., Green, M., Zwald, D., Purro, M., Schmid, J., Biffiger, K., Power, A. M., Oesch, B., Raeber, A. J., and Telling, G. C. (2005) Immunodetection of disease-associated mutant PrP, which accelerates disease in GSS transgenic mice, *EMBO J. 24*, 2472−2478.
35. Hornemann, S., Korth, C., Oesch, B., Riek, R., Wider, G., Wuthrich, K., and Glockshuber, R. (1997) Recombinant full-length murine prion protein, mPrP(23−231): Purification and spectroscopic characterization, *FEBS Lett. 413*, 277−281.
36. Pan, T., Li, R., Kang, S. C., Wong, B. S., Wisniewski, T., and Sy, M. S. (2004) Epitope scanning reveals gain and loss of strain specific antibody binding epitopes associated with the conversion of normal cellular prion to scrapie prion, *J. Neurochem. 90*, 1205−1217.
37. Pan, T., Wong, P., Chang, B., Li, C., Li, R., Kang, S. C., Wisniewski, T., and Sy, M. S. (2005) Biochemical fingerprints of prion infection: Accumulations of aberrant full-length and N-terminally truncated PrP species are common features in mouse prion disease, *J. Virol. 79*, 934−943.
38. Kazlauskaite, J., and Pinheiro, T. J. (2005) Aggregation and fibrillization of prions in lipid membranes, *Biochem. Soc. Symp.*, 211−222.
39. Bocharova, O. V., Makarava, N., Breydo, L., Anderson, M., Salnikov, V. V., and Baskakov, I. V. (2006) Annealing prion protein amyloid fibrils at high temperature results in extension of a proteinase K-resistant core, *J. Biol. Chem. 281*, 2373−2379.
40. Prusiner, S. B., McKinley, M. P., Bowman, K. A., Bolton, D. C., Bendheim, P. E., Groth, D. F., and Glenner, G. G. (1983) Scrapie prions aggregate to form amyloid-like birefringent rods, *Cell 35*, 349−358.
41. McKinley, M. P., Meyer, R. K., Kenaga, L., Rahbar, F., Cotter, R., Serban, A., and Prusiner, S. B. (1991) Scrapie prion rod formation in vitro requires both detergent extraction and limited proteolysis, *J. Virol. 65*, 1340−1351.
42. Silveira, J. R., Raymond, G. J., Hughson, A. G., Race, R. E., Sim, V. L., Hayes, S. F., and Caughey, B. (2005) The most infectious prion protein particles, *Nature 437*, 257−261.
43. Hegde, R. S., Mastrianni, J. A., Scott, M. R., DeFea, K. A., Tremblay, P., Torchia, M., DeArmond, S. J., Prusiner, S. B., and Lingappa, V. R. (1998) A transmembrane form of the prion protein in neurodegenerative disease, *Science 279*, 827−834.
44. Falnes, P. O., and Sandvig, K. (2000) Penetration of protein toxins into cells, *Curr. Opin. Cell Biol. 12*, 407−413.
45. Nishina, K., Deleault, N. R., Lucassen, R. W., and Supattapone, S. (2004) In vitro prion protein conversion in detergent-solubilized membranes, *Biochemistry 43*, 2613−2621.
46. Saborio, G. P., Permanne, B., and Soto, C. (2001) Sensitive detection of pathological prion protein by cyclic amplification of protein misfolding, *Nature 411*, 810−813.
47. Klein, T. R., Kirsch, D., Kaufmann, R., and Riesner, D. (1998) Prion rods contain small amounts of two host sphingolipids as revealed by thin-layer chromatography and mass spectrometry, *Biol. Chem. 379*, 655−666.
48. Deleault, N. R., Lucassen, R. W., and Supattapone, S. (2003) RNA molecules stimulate prion protein conversion, *Nature 425*, 717−720.
49. Deleault, N. R., Geoghegan, J. C., Nishina, K., Kascsak, R., Williamson, R. A., and Supattapone, S. (2005) Protease-resistant prion protein amplification reconstituted with partially purified substrates and synthetic polyanions, *J. Biol. Chem. 280*, 26873−26879.
50. Xiong, L. W., Raymond, L. D., Hayes, S. F., Raymond, G. J., and Caughey, B. (2001) Conformational change, aggregation and fibril formation induced by detergent treatments of cellular prion protein, *J. Neurochem. 79*, 669−678.
51. Leffers, K. W., Wille, H., Stohr, J., Junger, E., Prusiner, S. B., and Riesner, D. (2005) Assembly of natural and recombinant prion protein into fibrils, *Biol. Chem. 386*, 569−580.
52. Polymenidou, M., Stoeck, K., Glatzel, M., Vey, M., Bellon, A., and Aguzzi, A. (2005) Coexistence of multiple PrPSc types in individuals with Creutzfeldt-Jakob disease, *Lancet Neurol. 4*, 805−814.

BI700299H